RESEARCH ARTICLE SUMMARY

SUPERCONDUCTIVITY

Coexistence of superconductivity with partially filled stripes in the Hubbard model

Hao Xu†, Chia-Min Chung†, Mingpu Qin, Ulrich Schollwöck, Steven R. White, Shiwei Zhang*

INTRODUCTION: An iconic model in quantum many-body physics, the Hubbard model has been intensely studied. Since the discovery of high-temperature cuprate superconductors, a central question has been whether the two-dimensional (2D) Hubbard model qualitatively captures the essential physics of these materials. Answering this question has proved to be especially difficult because the ground state of the model has been shown to be exceptionally sensitive to small changes in the model terms and parameters. The relevant model parameters are in the most difficult regime—moderately strongly coupled—where most approaches struggle. The frequent presence of stripes in the ground states increases the sizes of the clusters needed to extrapolate to the thermodynamic limit.

A powerful tool has emerged to help overcome these difficulties: the use of combinations of simulation methods with complementary strengths and weaknesses. For example, the constrained path (CP) auxiliary field quantum Monte Carlo (AFQMC) and the density-matrix renormalization group (DMRG) were used to study the pure (i.e., with no next-nearest-neighbor hopping) Hubbard model. It was found that superconductivity is absent in the ground state. In that case, the lack of superconductivity was tied to the occurrence of filled-striped states.

We applied this approach to tackle the ground states of the 2D Hubbard model with next-nearest-neighbor hopping, t'. In connection with the typical phase diagram of cuprates, a t' is needed to account for the particle-hole asymmetry and band structures. The presence of t' turns out to substantially magnify the sensitivities in the model and make it more challenging to perform accurate computations and reliable extrapolations to the thermodynamic limit.

RATIONALE: We used two powerful modern computational methods, DMRG and CP AFQMC, which are particularly complementary to each other. DMRG provides the most accurate and reliable results when applied on narrow cylinders. CP AFQMC can be applied to both wider cylinders and toruses. The underlying approximation of CP is unrelated to the low-entanglement approximation of DMRG. AFQMC is based on a wave picture, whereas DMRG is rooted in the particle picture. Their quantitative "handshake" proved crucial for uncovering the delicate nature of the stripe correlations. The use of twist-averaged boundary conditions, which effectively sample the low-lying states, provided another key ingredient. Reaching wider cylinders and large toruses allowed extrapolation to the thermodynamic limit.

RESULTS: We found superconductivity in both the electron- and hole-doped regimes. The ground-state pairing-order parameter, which we expected to be loosely connected to the transition temperature (T_c) most readily observed experimentally, displayed dome-like structures as a function of doping, resembling the T_c domes of the cuprates. The pairing-order parameter was considerably larger in the hole-doped region than in the electron-doped region. On the hole-doped side, we found the coexistence of superconductivity with fractionally filled stripe correlations, with nominal stripe fillings in the range 0.6 to 0.8 in sufficiently large system sizes. On the electron-doped side, at lower dopings, uniform or weakly modulated antiferromagnetism—along with uniform or weakly modulated doping—coexisted with somewhat-weaker superconductivity. These behaviors of spin and charge are again consistent with the phase diagram of the cuprates, in which uniform antiferromagnetic correlations persist with substantial doping on the electron-doped side but short- or long-ranged incommensurate magnetism and stripes are observed starting at small doping on the hole-doped side. The general appearance of stripe orders on the larger systems with non-integral numbers of pairs indicates that pairs fluctuate between stripes, promoting long-distance phase coherence and thus superconductivity.

CONCLUSION: Can the single-band Hubbard model capture the qualitative physics—particularly the superconductivity—of the cuprates? Our calculations suggest that the answer is "yes"—that the Hubbard model with a next-nearest-neighbor hopping t' distinguishing between electron doping and hole doping captures the essential features of the charge, magnetic, and pairing orders. Other terms and effects not present in the Hubbard model may still play important quantitative roles. Nevertheless, it appears that qualitatively, the t-t'-U Hubbard model may have "the right stuff." ■

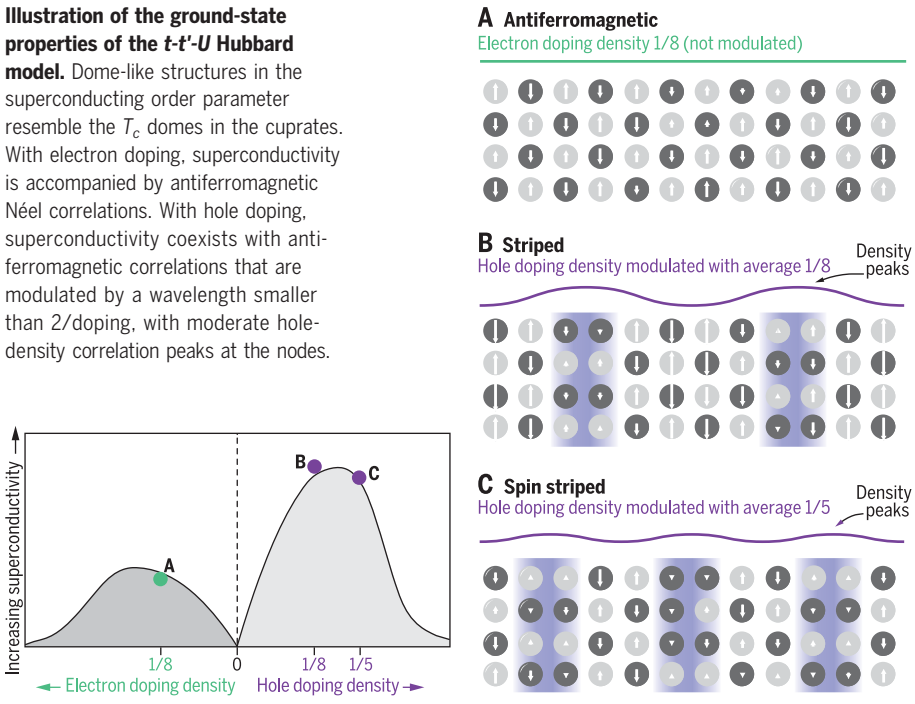

Illustration of the ground-state properties of the t-t'-U Hubbard model. Dome-like structures in the superconducting order parameter resemble the T_c domes in the cuprates. With electron doping, superconductivity is accompanied by antiferromagnetic Néel correlations. With hole doping, superconductivity coexists with antiferromagnetic correlations that are modulated by a wavelength smaller than 2/doping, with moderate hole-density correlation peaks at the nodes.

The list of author affiliations is available in the full article online.
*Corresponding author. Email: szhang@flatironinstitute.org
†These authors contributed equally to this work.
Cite this article as H. Xu *et al.*, *Science* **384**, eadh7691 (2024). DOI: 10.1126/science.adh7691

READ THE FULL ARTICLE AT
https://doi.org/10.1126/science.adh7691

RESEARCH ARTICLE

SUPERCONDUCTIVITY

Coexistence of superconductivity with partially filled stripes in the Hubbard model

Hao Xu[1]†, Chia-Min Chung[2,3,4]†, Mingpu Qin[5,6], Ulrich Schollwöck[7,8], Steven R. White[9], Shiwei Zhang[10]*

The Hubbard model is an iconic model in quantum many-body physics and has been intensely studied, especially since the discovery of high-temperature cuprate superconductors. Combining the complementary capabilities of two computational methods, we found superconductivity in both the electron- and hole-doped regimes of the two-dimensional Hubbard model with next-nearest-neighbor hopping. In the electron-doped regime, superconductivity was weaker and was accompanied by antiferromagnetic Néel correlations at low doping. The strong superconductivity on the hole-doped side coexisted with stripe order, which persisted into the overdoped region with weaker hole-density modulation. These stripe orders varied in fillings between 0.6 and 0.8. Our results suggest the applicability of the Hubbard model with next-nearest hopping for describing cuprate high–transition temperature (T_c) superconductivity.

Does the Hubbard model qualitatively capture the essential physics of the high-temperature superconducting cuprates? This question has been debated since shortly after these materials were discovered (*1*–*10*). Answering it has proved to be especially difficult because the ground states of the models have been shown to be exceptionally sensitive to small changes in the model terms and parameters, with competing (*11*) or cooperating (*12*) charge, spin (*13*), and superconducting orders (*14*–*18*). The relevant model parameters are in the most difficult regime—moderately strongly coupled—where most approaches struggle. The frequent presence of stripes in the ground states increases the sizes of the clusters needed to extrapolate to the thermodynamic limit.

A powerful tool has emerged to help overcome these difficulties: the use of combinations of simulation methods with complementary strengths and weaknesses (*19*). The density-matrix renormalization group (DMRG) (*20*–*22*) provides the most accurate and reliable results when applied on fairly narrow cylinders (*23*). Other methods work either directly in the thermodynamic limit (*24*, *25*) or at least on much wider clusters as compared with DMRG (*26*), but these methods have approximations tied to unit-cell size (*24*, *27*, *28*), coupling strength, and other factors (*25*, *29*, *30*). The constrained path (CP) auxiliary-field quantum Monte Carlo (AFQMC) method (*26*, *31*, *32*) is particularly complementary to DMRG: It can be applied to both wider cylinders and toruses (supercells periodic in both directions); the errors from CP to control the sign problem have been consistently modest (*19*), and the underlying approximation of CP is unrelated to the low-entanglement approximation of DMRG. AFQMC is based on a wave picture of superpositions of Slater determinants, whereas DMRG is rooted in the particle picture with strong coupling. The quantitative "handshake" of these two methods proved to be crucial for uncovering the delicate nature of the stripe correlations, as we discuss below. Previously, this combination was used by extrapolating to the two-dimensional thermodynamic limit to find that superconductivity is absent in the pure (with no next-nearest-neighbor hopping) Hubbard model (*11*). In that case, the lack of superconductivity was tied to the occurrence of filled-stripe states (*33*).

In this study, we refined this approach to tackle the Hubbard model with a nonzero next-nearest-neighbor hopping, t'. In connection to the typical phase diagram of cuprates, a nonzero t' is necessary to account for the particle-hole asymmetry and the band structures. The $t' \neq 0$ model is considerably more difficult computationally, with challenges for both DMRG and AFQMC. In situations for which both methods apply, we used DMRG to certify the high accuracy and reliability of our AFQMC calculations. In cases of ambiguity (e.g., in some width-6 cylinders), resolving the discrepancies contributed to growing synergy between the two methods and led to additional physical insights. We have found that the phase diagram with finite t' is a great deal more complicated than for the pure Hubbard model and features partially filled stripes coexisting with superconductivity on the hole-doped side and uniform antiferromagnetic (AFM) order coexisting with superconductivity on the electron side. The final results for superconductivity, extrapolated to the thermodynamic limit, are similar to the properties of cuprates, with both electron- and hole-doped superconducting "domes," but with the hole-doped side dome being much taller.

Hubbard model and lattice geometry

The Hamiltonian of the Hubbard model is

$$\hat{H} = -t\sum_{\langle ij\rangle,\sigma} \hat{c}^{\dagger}_{i\sigma}\hat{c}_{j\sigma} - t'\sum_{\langle\langle ij\rangle\rangle,\sigma} \hat{c}^{\dagger}_{i\sigma}\hat{c}_{j\sigma} + U\sum_{i} \hat{n}_{i\uparrow}\hat{n}_{i\downarrow} - \mu\sum_{i\sigma} \hat{n}_{i\sigma}, \quad (1)$$

where i or j labels a site on a square lattice, $\hat{c}^{\dagger}_{i\sigma}$ is the electron creation operator, $\sigma = \{\uparrow, \downarrow\}$ denotes spin, $\hat{n}_{i\sigma} = \hat{c}^{\dagger}_{i\sigma}\hat{c}_{i\sigma}$ is the particle-number operator, and $\langle ij\rangle$ and $\langle\langle ij\rangle\rangle$ indicate nearest and next-nearest neighbors, respectively. We set t as the energy unit. In cuprates, $t' < 0$ (*34*); however, using a particle-hole transformation to map fillings $1 + \delta \rightarrow 1 - \delta$, we can study electron doping by changing the sign of t'. We used $t' = -0.2$ for hole doping and $t' = +0.2$ for electron doping, according to band-structure calculations in cuprates (*35*, *36*). The on-site repulsion U was fixed at $U = 8$, again a representative value for cuprates. We scanned a range of doping (denoted by δ) by varying μ.

Our study focused on the ground state, which we obtain in either cylindrical or toric systems. The use of cylinders serves two purposes. First, they allow direct comparisons between AFQMC and DMRG, which is highly accurate in narrow cylinders. Second, they are convenient for studying spin and charge orders, in which we applied spin symmetry–breaking pinning fields on the edges of the cylinder to help detect ordering from the resulting local spin and charge densities. The calculations in toruses allow AFQMC to better approach the thermodynamic limit (TDL). As shown below, it turned out to be crucial to systematically average over different boundary conditions. To compute the pairing-order parameter, we applied twist-averaged boundary conditions (TABC) over a large number of random twists in systems with up to 500 lattice sites. We discuss the improvements to the capability and accuracy of the two methods that enabled this study in several of the following sections.

[1]Department of Physics, College of William and Mary, Williamsburg, VA 23187, USA. [2]Department of Physics, National Sun Yat-sen University, Kaohsiung 80424, Taiwan. [3]Center for Theoretical and Computational Physics, National Sun Yat-sen University, Kaohsiung 80424, Taiwan. [4]Physics Division, National Center for Theoretical Sciences, Taipei 10617, Taiwan. [5]Key Laboratory of Artificial Structures and Quantum Control, School of Physics and Astronomy, Shanghai Jiao Tong University, Shanghai 200240, China. [6]Hefei National Laboratory, Hefei 230088, China. [7]Arnold Sommerfeld Center for Theoretical Physics, Ludwig-Maximilians-Universität München, 80333 Munich, Germany. [8]Munich Center for Quantum Science and Technology (MCQST), 80799 Munich, Germany. [9]Department of Physics and Astronomy, University of California, Irvine, CA 92697, USA. [10]Center for Computational Quantum Physics, Flatiron Institute, New York, NY 10010, USA.
***Corresponding author. Email: szhang@flatironinstitute.org**
†These authors contributed equally to this work.

Overview of pairing and coexisting spin and charge orders

Figure 1 presents an overview of our results, a "phase diagram" of the computed pairing-order parameter, together with representative spin and charge correlations. The pairing-order parameter Δ_d we computed is the expectation value of the operator $\sum_{\langle ij \rangle} \left[b_{ij} \left(\hat{\Delta}_{ij} + \hat{\Delta}_{ij}^{\dagger} \right) / 2 \right]$, where $\hat{\Delta}_{ij} \equiv \left(\hat{c}_{i\uparrow} \hat{c}_{j\downarrow} - \hat{c}_{i\downarrow} \hat{c}_{j\uparrow} \right) / \sqrt{2}$ and $b_{ij} = +1$ if the bond $\langle ij \rangle$ is in the x direction and $b_{ij} = -1$ if $\langle ij \rangle$ is in the y direction. The pairing-order parameters have been extrapolated to the TDL, using full TABC in large simulation cells [see below and (*37*)]. We would expect this zero-temperature property to be loosely connected to the transition temperature (T_c) most readily observed experimentally [however, see (*38*, *39*)]. On both the electron- and hole-doped sides, we find dome-like d-wave pairing orders that resemble the T_c domes in the typical phase diagram of cuprates. The pairing-order parameter is substantially larger in the hole-doped region than in the electron-doped region, which is also consistent with the phase diagram of cuprates (*40*).

Spin and hole densities are shown for the three representative systems marked as A, B, and C. These calculations were performed with AFM pinning fields on the edges of the cylindrical simulation cells (*37*). The spin and hole densities thus provide a simple and convenient way to visualize the spin and charge correlations. We have taken care to ensure that the results are drawn from very large systems and that the spin and charge patterns are representative of different boundary conditions. In the electron-doped region, the spins show single-domain antiferromagnetism with nearly uniform hole densities in the bulk. In the hole-doped region, stripe and spin-density wave (SDW) correlations are observed, with modulated AFM domains separated by phase-flip lines where holes are more concentrated. In contrast with the pure Hubbard model, we found that the wavelength of the modulation is not an integer multiple of 1/δ (filled stripes). Nor are the stripes half-filled as seen in previous state-of-the-art calculations (*41*). Rather, they are best described as partially filled, with fractional fillings that vary with δ as well as system-size and boundary conditions. These behaviors of spin and charge are again consistent with the phase diagram of the cuprates (*40*), in which uniform AFM correlations persist with substantial doping on the electron-doped side but short or long-ranged incommensurate magnetism and stripes are observed starting at small doping on the hole-doped side (*42*, *43*).

It is instructive to consider this phase diagram in the context of the t-t'-J model (*44*, *45*), which can be derived as an approximate strong-coupling Hubbard model at low doping. In the t-t'-J model, recent DMRG studies all point to strong d-wave superconductivity on the electron-doped side (*44*–*46*), which coexists with AFM correlations with increasing strength as t' increases; some differences remain concerning whether long-range AFM order occurs (*47*). To date, indications are that superconductivity is weak or marginal on the hole-doped side

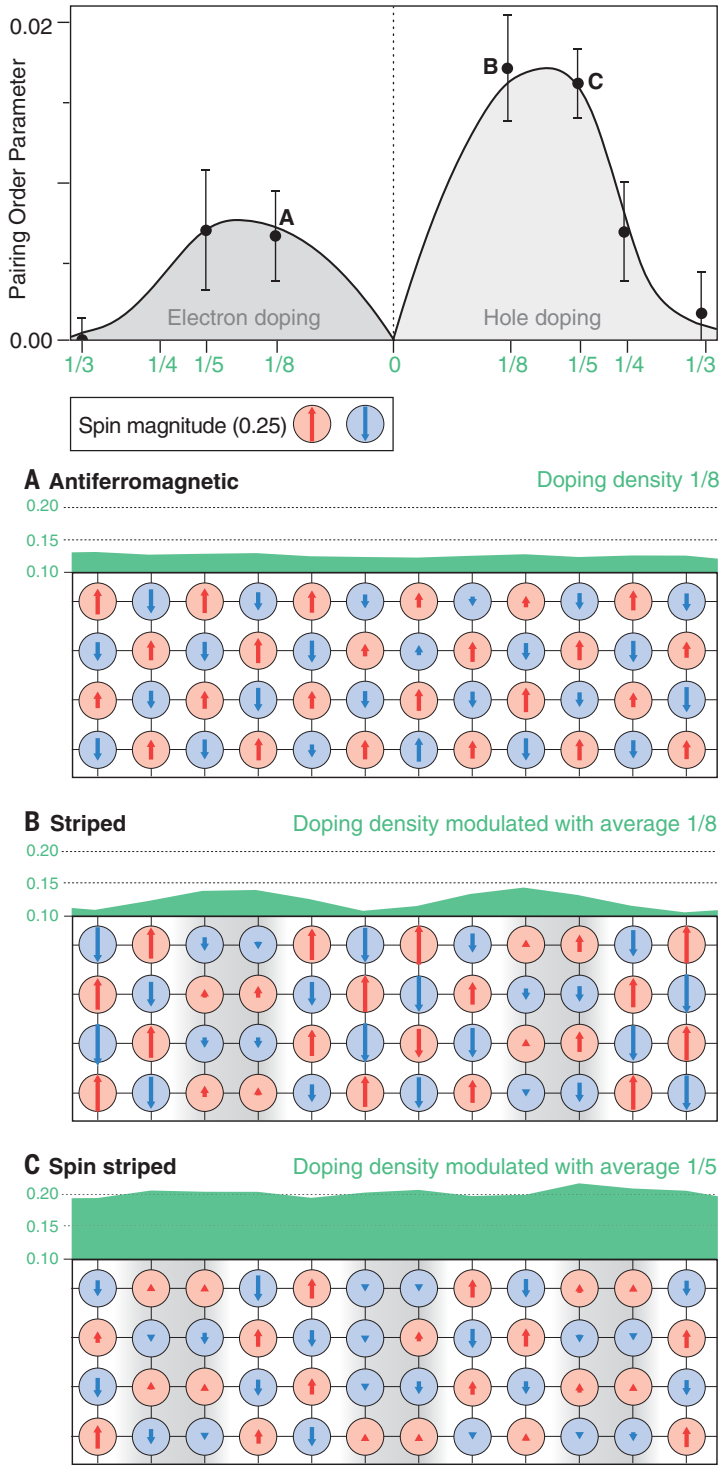

Fig. 1. The d-wave pairing-order parameter as a function of doping δ. Shown is the ground state for the hole-doped ($t' = -0.2$) and electron-doped ($t' = +0.2$) regimes. Representative spin and charge correlations are also shown for three parameter sets: A, B, and C. Δ_d is the spontaneous pairing order in the thermodynamic limit; the spin and charge (hole) patterns are drawn from the middle of 28 by 8 (A), 24 by 8 (B), and 40 by 8 (C) cylinders with AFM-spin pinning fields applied to the two edges. The vertical scale for the hole-density plots (top of panels A, B, and C) starts at 0.1. Gray shadows for spins are to aid the eye.

(*44*, *48*). Is this difference caused by the strong-coupling approximations of that model, or by other flaws or missing terms affecting both the Hubbard and *t*-*t*′-*J* (single-band) models? Our results point to the former. These differences have not been clear in previous studies on narrower cylinders, which are impacted by strong finite-size effects (*49*, *50*).

Underdoped region: 1/8 hole doping

A relatively large pairing-order parameter is found in this region, in coexistence with stripe correlations (Fig. 1). To better understand the nature of the spin and charge correlations, we systematically studied their evolution with system sizes, as shown in Fig. 2. The computations were performed in $L_x \times L_y$ cells, with periodic boundary condition (PBC) or antiperiodic boundary condition (APBC) in the $\hat{y}$ direction and open BC along $\hat{x}$ (i.e., cylinders). AFM pinning fields (along $\hat{z}$) were applied at $x = 1$ and L_x to break the SU(2) symmetry and induce local spin orders, such that the local spin density, $S_z(x, y)$, becomes a proxy of spin-spin correlations away from the edges of the cylinder.

Modulated AFM patterns are clearly seen in all the systems. Correspondingly, hole densities are enhanced at the nodes of the spin modulation (Fig. 1) [results on the corresponding hole densities for Fig. 2 can be found in fig. S4 in (*37*)]. The characteristic wavelength of the modulation, λ_{SDW}, varies with system size. We define a filling fraction of the stripe as $f \equiv \delta\lambda_{SDW}/2$, i.e., the number of holes per lattice spacing along a stripe. In the pure Hubbard model, $f = 1$ because $\lambda_{SDW} = 2/\delta$ (*51*, *52*). Then, nominally the number of electron pairs per stripe is $n_p \equiv f\ L_y/2$. If n_p is an integer, we refer to the state as integer-pair stripe (IPS); otherwise the state is labeled as non-IPS (NIPS).

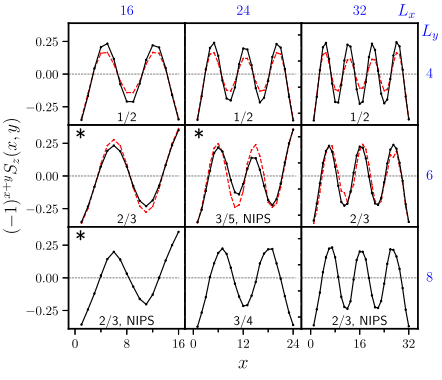

Fig. 2. Evolution of the stripe patterns with system size (δ = 1/8, hole-doped). The staggered spin densities are shown as linecuts in periodic cylinders. The length of the cylinder (L_x) is varied across the three columns and the width (L_y) across rows. AFM pinning fields are applied at the two edges of the cylinder ($x = 1$ and $x = L_x$), either in phase or with a π-phase shift (marked by an asterisk); the state with lower energy is shown. The filling fraction *f* of each stripe pattern is indicated, with NIPS denoting noninteger-pair stripes. DMRG results (red) are shown for width-4 and width-6 systems, and AFQMC results (black) are in good agreement with them.

Previous studies in width-4 cylinders have found that the ground state in this system has half-filled stripes (*41*, *44*, *45*). Our results confirm this picture, with good agreement between AFQMC and DMRG, but also show that the half-filled stripe turns out to be special to width-4. As the system size increases, the stripe filling fluctuates between 3/5 and 3/4; NIPS states appear frequently. Previous calculations (*11*, *53*) show that states with IPS are favored, which was taken as an indication of the existence of local pairing of electrons in the stripe state. Our results indicate that, with the inclusion of *t*′, the electron is more mobile and pairs of electrons become coherent, displaying long-range pairing order. This is further discussed and contrasted with the overdoped region in the next section.

Overdoped region: 1/5 hole doping

A strong superconducting order parameter is found in the ground state of the hole-overdoped region of δ = 1/5, with strength comparable to δ = 1/8 (Fig. 1). The behavior of spin and charge correlations shows common features but also considerable differences between the two regions. Figure 3 summarizes their stripe fillings side by side, from computations in about 30 systems. Several trends are evident. In narrow cylinders, IPS states are favored at both dopings. In more than a dozen different width-4 and width-6 systems across the two dopings, AFQMC and DMRG agree in each case on the stripe wavelength and filling fraction. In both regimes, the filling fraction varies widely with system sizes and boundary conditions, and fluctuations continue through systems with over 500 lattice sites. As the size grows (wider cylinders), IPS states are no longer favored and both systems tend to fractional stripe fillings. These results indicate that with *t*′, the stripe patterns—but not the existence of stripes—are much more fragile than in the pure Hubbard model.

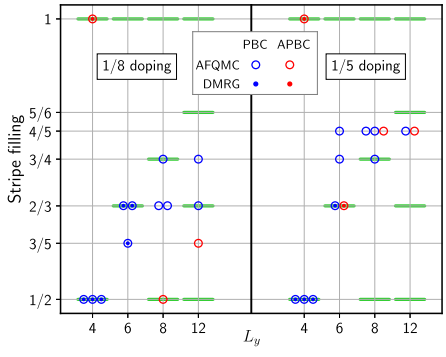

Fig. 3. Partially filled stripe patterns on the hole-doped side, at δ = 1/8 and 1/5. The stripe fillings are shown for a variety of system sizes, in cylindrical cells with width $L_y = 4$ up to 12, and lengths ranging from 16 to 48. The L_x value of each symbol is provided in table S1. Results for both PBC and APBC are shown. Narrow cylinders favor integer-pair stripes (IPS, indicated by green bars). Fluctuations are strong even in large systems.

Both the spin and charge modulations are weaker at 1/5 doping than at 1/8. Although *f* is larger in the TDL, the holes are more mobile and spread out in the overdoped region. The hole density is nearly uniform, with less than 5% of the holes contributing to the density fluctuations. At 1/8 doping, the stripe order is more pronounced (Fig. 1). Nevertheless, the peak density of holes at the nodes of the spin correlation is only ~30% higher than the average. The notion of stripe filling derives from a particle picture, most applicable to holes in Wigner crystal–like distributions. The holes in the systems studied here have a strong wave character (*51*), with which the fractional fillings of stripes that we observed are more readily compatible.

Electron-doped region

Experimentally, the electron-doped side is simpler, without the competing stripe state (*42*, *54*) or pseudogap phase in cuprates (*40*). The critical doping for the long-range AFM order on the electron-doped side is larger than that on the hole-doped side, the superconducting dome is smaller, and the transition temperature is lower. The phase diagram in Fig. 1 and the spin and hole densities in Fig. 4 are consistent with these features.

Our results reveal several other important features on the electron-doped side. There are considerable variations of the spin and charge correlations with system sizes and boundary conditions, even though the sensitivity is less compared with the hole-doped side. Two entirely different ground-state orders are obtained from width-4 and width-6 cylinders (fig. S2), and APBC and PBC also lead to opposite conclusions in each simulation cell. Even in the width-8 systems in Fig. 4, which display robust Néel order, different boundary conditions still show variations in the charge correlation. Superconductivity manifests a more dramatic volatility; using PBC, the most common approach to date, calculations in width-4 and width-6 cylinders would yield a strong pairing order in the electron-doped regime. (DMRG and AFQMC give fully consistent results.) By contrast, under APBC the same calculations predict no pairing. The uncertainties with respect to finite size and boundary conditions are much larger than the final signal at the TDL. Thus, even a qualitative conclusion on superconductivity would be challenging without using TABC, systematic extrapolation to large sizes, and other

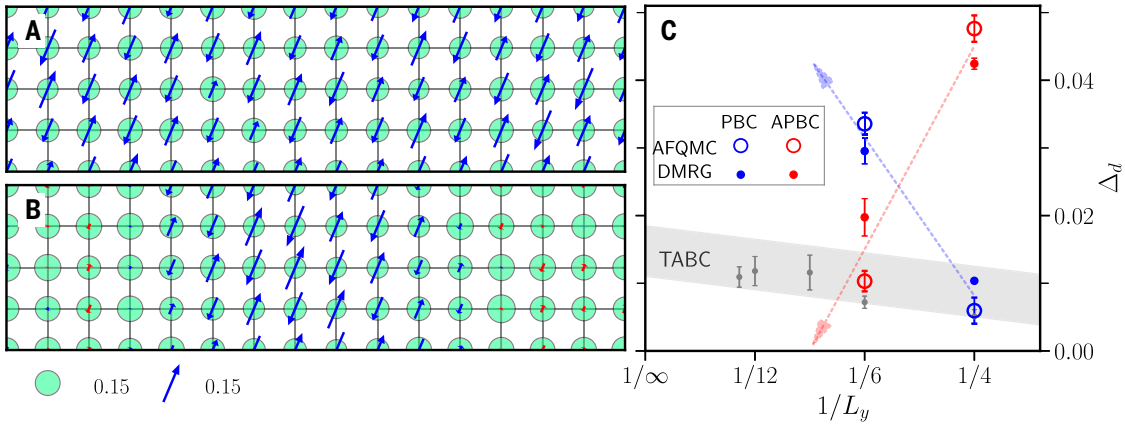

Fig. 4. Spin, charge, and pairing properties on the electron-doped side (δ = 1/8). Note their variations with boundary conditions. (**A**) APBC along $\hat{y}$ direction in a 28 by 8 cylinder gives nearly uniform Néel order (only a 16 by 4 central region is shown). (**B**) Under PBC, a modulated AFM order with larger spatial variations in spin magnitude is seen. (**C**) The computed pairing orders in 16 by 4 and 16 by 6 cylinders (at a fixed value $h_d = 0.021$ of applied global d-wave pairing fields) show opposite trends with PBC and APBC. The final pairing order, computed from TABC in large toruses of increasing L_y, is shown together with the TDL extrapolation by the gray band.

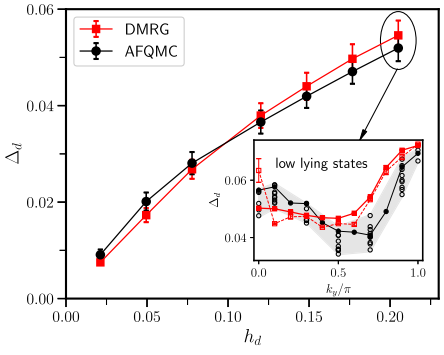

Fig. 5. Importance of TABC for accurate determination of the pairing order. The main figure shows the d-wave pairing-order parameters in a 20 by 4 cylindrical cell at 1/5 hole doping, after full twist averaging over k_y. AFQMC and DMRG results agree across the entire range of the applied pairing field h_d. (Inset) The inset focuses on $h_d = 0.205$. Δ_d computed from DMRG and AFQMC are shown as a function of k_y, for the ground state (connected by solid line) and some of the lowest-lying excited states (open symbols). Averages of the solid symbols lead to the TABC results in the main figure.

methodological advances, which are discussed in the next sections.

Twist averaging as an effective means to sample low-lying states

The use of twist averaging (*55*, *56*) in this work had two crucial roles. First, systematically averaging over twist angles, combined with the ability to reach large system sizes and careful finite-size extrapolation, enabled us to approach the TDL reliably. Second, the random twist angles provided an effective means to sample the low-lying states, and their averaging reduced the impact of rare events of accidental degeneracy and smoothed out the effect of level crossings as a function of an applied pairing field (*37*).

Different boundary conditions can result in variations in the pairing-order parameter that are many times larger than the signal, even in nominally rather large sizes (width-6 cylinders) (Fig. 4). Both PBC and APBC are twist angles of special symmetry and are often particularly volatile. The twisted boundary condition (TBC) can be thought of as the electron gaining a phase when it crosses the boundary. Equivalently, we can choose another gauge by distributing the phase evenly in each hopping term. When a twist is applied, care must be taken in defining the pairing-order parameter, whose form is gauge-dependent but whose expectation value should be gauge-independent (*37*). We applied TABC with quasi-random twist angles (*56*). TABC reduces the fluctuations in the computed pairing-order parameter (Fig. 4) [also discussed further below and in (*37*)]. TBC and twist averaging have been shown to accelerate the extrapolation with calculations on cylinders (*57*).

With the inclusion of a nonzero t', the perfect nesting in the Fermi surface at half-filling is absent. Subtle variations near the Fermi level from finite size and boundary conditions can have a much larger effect on the formation of collective spin modes, thus there is more sensitivity in the property of the low-lying states. These states can be extremely close in energy such that any small finite temperature (e.g., under experimental conditions) would smear them out and render them indistinguishable. TABC provides an effective sampling of such low-lying states, which can average out the fluctuations so as to more reliably capture the intrinsic properties (Fig. 5). The pairing-order parameter exhibits large variations as a function of the twist angle, both in the ground state and low-lying excited states, as seen in the inset for one value of h_d (the magnitude of the applied pairing field). The calculation can "hop" from one state to another among the bundle of low-lying states, depending on the initial condition, convergence criterion, and other factors, even under high-quality computational settings (e.g., large bond dimensions in DMRG). This is also reflected in the modest level of agreement between the two methods for each particular state. With TABC, however, their agreement is excellent across the entire range of h_d [which spans many level crossings (*37*)], and the two methods give fully consistent conclusions.

Extrapolation of pairing order

The spontaneous pairing-order parameter in the TDL, Δ_d, was obtained from a massive number of computations. Each calculation was performed in the presence of a small but finite global pairing field, h_d (*37*). At each parameter set (t' and doping), $\Delta_d(N, h_d)$ was computed for many different simulation-cell sizes, N, at tens of h_d values, with each averaged over tens of quasi-random twist angles. We then took the limit $\Delta_d(N\to\infty, h_d)$ at each h_d, followed by the extrapolation $\Delta_d(\infty, h_d\to 0)$ (Fig. 6). Figure 6A shows the first step, in which we used $N = L_x \times L_y$ supercells (toruses) with quasi-random twist angles (k_x, k_y) applied to both directions. We verified that L_x is sufficiently large such that the results converged within our statistical accuracy. We then extrapolated the TABC results with respect to $1/L_y$, excluding small sizes. [Deviations are visible from width-4 systems, which can have different pairing symmetry from ordinary d-wave pairing (*50*).] As shown in Fig. 6B, extrapolations were then performed using small h_d values (<0.05 for linear and last 10 or so points for quadratic fits),

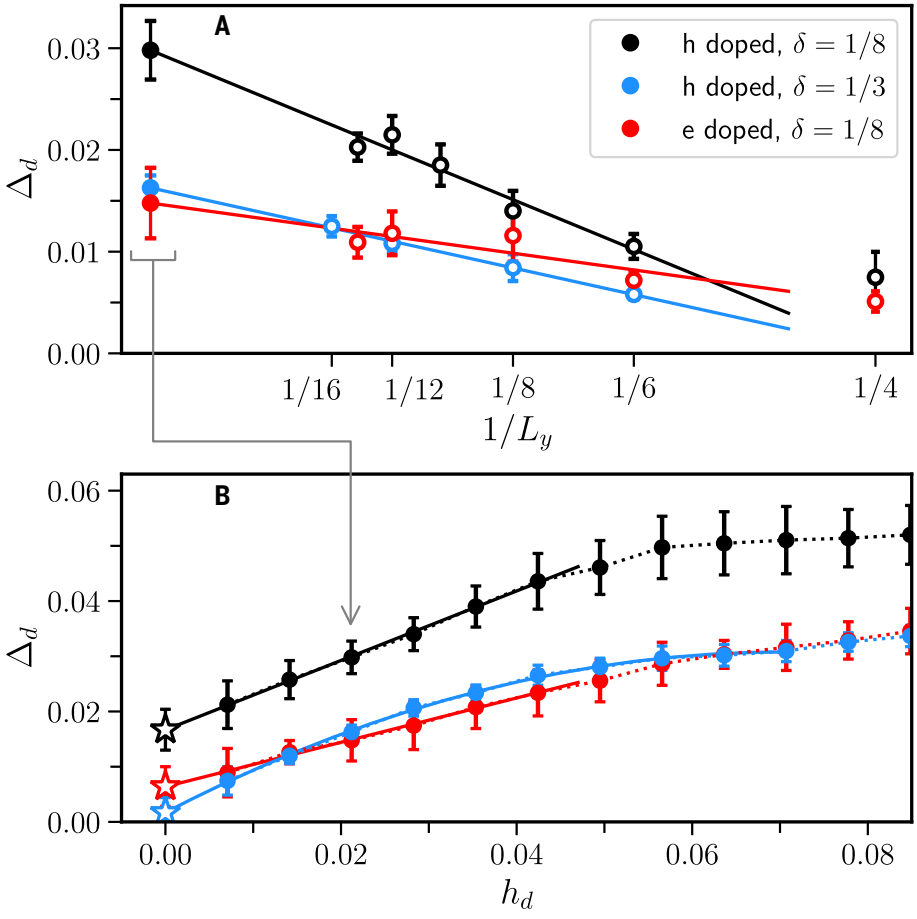

Fig. 6. Computation of the ground-state pairing-order parameter at the thermodynamic limit. (**A**) Extrapolation to the TDL at a fixed h_d, the strength of the *d*-wave pairing fields. (**B**) Extrapolation of the TDL result from (A) to $h_d \to 0$. Three representative systems are shown. In (A), each data point is obtained by TABC over (k_x, k_y) in supercells of $L_x \times L_y$, and only results from large supercells are included. In (B), linear or quadratic fits are performed (full lines) at small values of h_d, with extrapolated values marked as stars; the dashed lines connect the data points to guide the eye.

yielding the final spontaneous pairing-order parameter Δ_d at $h_d \to 0$. As can be seen, the quality of the fits is excellent; in each case, the linear and quadratic fits give consistent values within statistical errors. The pairing-order parameters shown in Fig. 1 are the final Δ_d after extrapolations to the TDL, and then to the zero–pairing field limit.

Discussion and outlook

Can the single-band Hubbard model capture the qualitative physics—particularly the superconductivity—of the cuprates? Our calculations suggest that the answer is "yes"—that the Hubbard model with a next-nearest-neighbor hopping t' distinguishing between electron doping and hole doping captures the essential features of the charge, magnetic, and pairing orders.

The computed pairing-order parameter in the ground state as a function of doping displays dome-like structures resembling the T_c domes of the cuprates. On the hole-doped side, we found the coexistence of superconductivity with fractionally filled stripe correlations, with nominal stripe fillings in the range 0.6 to 0.8 in sufficiently large sizes. On the electron-doped side, at lower dopings, we found that uniform or weakly modulated antiferromagnetism—along with uniform or weakly modulated doping—coexisted with somewhat weaker superconductivity. The general appearance of stripe orders on the larger systems with nonintegral numbers of pairs indicates that pairs fluctuate between stripes, promoting long-distance phase coherence and thus superconductivity; by contrast, for $t' = 0$, the stripes were filled and superconductivity was absent (*11*).

This picture is in contrast to that of the *t*-*t*′-*J* model, once thought to be leading to the same results as the Hubbard model, which appears to exhibit only weak or marginal superconductivity on the hole-doped side (*44*, *46*). The ground states of the models are not universal, and to capture the subtle interaction of the various intertwined orders requires both very careful finite-size extrapolation and very high accuracy and reliability in the simulation methods. Even within the single-band *t*-*t*′ Hubbard model, an enormous body of works exists, with widely varying and often conflicting results. Our results also explain why this has been the case: The model shows extreme sensitivity of the properties to finite sizes and boundary conditions and to any biases of approximate methods.

The challenge in treating the Hubbard model is magnified substantially with a nonzero t'. The difficulties include more sensitivity and stronger dependency on system size and boundary condition, as we have illustrated. In addition, t' turns out to affect the interplay between low-lying states in important ways. For instance, with $t' = 0$, stripe and superconductivity manifest as competing orders. Filled-stripe states are particularly stable, with nesting contributing a key factor. A nonzero t' affects the nesting condition (frustrates the Néel order) and alters the landscape of the low-lying states, thus demanding much higher resolution from the numerical methods.

In this work, we have combined DMRG and AFQMC, with DMRG benchmarking and validating the CP approximation in AFQMC on narrower systems, and the AFQMC being used to reach much larger systems. The improvements to finite-size extrapolations owing to the use of TABC, together with methodological advances, enhanced the resolution of the results.

In the models or parameter regimes on the hole-doped side where superconductivity is not present, we still found strong indications of paired holes. For example, if holes within stripes were not paired, one would expect to find single stripes having an odd number of holes in about half the systems, but instead only even numbers of holes in each stripe were found. Whether there is superconductivity or not seems tied to the properties of a pair, e.g., its effective mass, which is strongly influenced by model parameters such as t'. A heavy pair or a pair that interacts strongly with the magnetic degrees of freedom of the region around it is more likely to be locked up in a stripe, suppressing phase coherence. This model specificity and nonuniversality raises the question: Is there any simple analytic theory of cuprate superconductivity in the style of Bardeen-Cooper-Schrieffer (BCS), or must we always resort to simulation?

Our study still leaves much to do in connecting the models quantitatively to experiments. We have not predicted transition temperatures, only order parameters. We have not studied transport and dynamical properties of the models. Many other properties of the one-band Hubbard model remain to be determined and understood. Other terms (*58*, *59*) and effects not present in the Hubbard model may still play important quantitative roles. Nevertheless, it appears that qualitatively, the *t*-*t*′-*U* Hubbard model may have "the right stuff."

Methods summary

The methodologies used in this work have a number of distinguishing features that made it possible to improve accuracy and reliability. Two complementary, state-of-the-art computational methods were used synergistically. We implemented both U(1)- (*60*) and SU(2)-symmetry–adapted (*61*) DMRG calculations for different setups and pushed them to the large bond-dimension limit. In AFQMC, we introduced a further advance in the optimization of the constraining trial wave function [see fig. S1 in (*37*)], which is determined fully self-consistently (*32*) with no input parameter. Extensive and detailed comparisons between AFQMC and DMRG were performed on width-4 and width-6 cylinders, under identical conditions. The same AFQMC algorithm, which has no room for tuning, was applied to larger systems. The formulation of systematic twist averaging for the computation of the pairing-order parameters provides an effective way to sample the low-lying states.

REFERENCES AND NOTES

1. J. G. Bednorz, K. A. Müller, Possible highTc superconductivity in the Ba–La–Cu–O system. *Z. Phys. B Condens. Matter* **64**, 189 (1986). doi: 10.1007/BF01303701
2. J. Hubbard, Electron correlations in narrow energy bands. *Proc. R. Soc. Lond. Ser. A* **276**, 238–257 (1963). doi: 10.1098/rspa.1963.0204
3. P. W. Anderson, The Resonating Valence Bond State in La_2CuO_4 and Superconductivity. *Science* **235**, 1196–1198 (1987). doi: 10.1126/science.235.4793.1196; pmid: 17818979
4. V. J. Emery, Theory of high-Tc superconductivity in oxides. *Phys. Rev. Lett.* **58**, 2794–2797 (1987). doi: 10.1103/PhysRevLett.58.2794; pmid: 10034851
5. F. C. Zhang, T. M. Rice, Effective Hamiltonian for the superconducting Cu oxides. *Phys. Rev. B Condens. Matter* **37**, 3759–3761 (1988). doi: 10.1103/PhysRevB.37.3759; pmid: 9944993
6. P. W. Anderson, R. Schrieffer, A Dialogue on the Theory of High Tc. *Phys. Today* **44**, 54–61 (1991). doi: 10.1063/1.881261
7. E. Dagotto, Correlated electrons in high-temperature superconductors. *Rev. Mod. Phys.* **66**, 763–840 (1994). doi: 10.1103/RevModPhys.66.763
8. B. Keimer, S. A. Kivelson, M. R. Norman, S. Uchida, J. Zaanen, From quantum matter to high-temperature superconductivity in copper oxides. *Nature* **518**, 179–186 (2015). doi: 10.1038/nature14165; pmid: 25673411
9. M. Qin, T. Schäfer, S. Andergassen, P. Corboz, E. Gull, The Hubbard Model: A Computational Perspective. *Annu. Rev. Condens. Matter Phys.* **13**, 275–302 (2022). doi: 10.1146/annurev-conmatphys-090921-033948
10. D. P. Arovas, E. Berg, S. A. Kivelson, S. Raghu, The Hubbard Model. *Annu. Rev. Condens. Matter Phys.* **13**, 239–274 (2022). doi: 10.1146/annurev-conmatphys-031620-102024
11. M. Qin *et al.*, Absence of Superconductivity in the Pure Two-Dimensional Hubbard Model. *Phys. Rev. X* **10**, 031016 (2020). doi: 10.1103/PhysRevX.10.031016
12. H.-C. Jiang, S. A. Kivelson, Stripe order enhanced superconductivity in the Hubbard model. *Proc. Natl. Acad. Sci. U.S.A.* **119**, e2109406119 (2022). doi: 10.1073/pnas.2109406119; pmid: 34930822
13. S. R. White, D. J. Scalapino, Stripes on a 6-leg Hubbard ladder. *Phys. Rev. Lett.* **91**, 136403 (2003). doi: 10.1103/PhysRevLett.91.136403; pmid: 14525325
14. E. Gull, O. Parcollet, A. J. Millis, Superconductivity and the pseudogap in the two-dimensional Hubbard model. *Phys. Rev. Lett.* **110**, 216405 (2013). doi: 10.1103/PhysRevLett.110.216405; pmid: 23745902
15. A. S. Darmawan, Y. Nomura, Y. Yamaji, M. Imada, Stripe and superconducting order competing in the Hubbard model on a square lattice studied by a combined variational Monte Carlo and tensor network method. *Phys. Rev. B Condens. Matter* **98**, 205132 (2018). doi: 10.1103/PhysRevB.98.205132
16. A. Himeda, T. Kato, M. Ogata, Stripe states with spatially oscillating d-wave superconductivity in the two-dimensional t-t′-J model. *Phys. Rev. Lett.* **88**, 117001 (2002). doi: 10.1103/PhysRevLett.88.117001; pmid: 11909421
17. B. Ponsioen, S. S. Chung, P. Corboz, Period 4 stripe in the extended two-dimensional Hubbard model. *Phys. Rev. B Condens. Matter* **100**, 195141 (2019). doi: 10.1103/PhysRevB.100.195141
18. P. Corboz, T. M. Rice, M. Troyer, Competing states in the t-J model: Uniform D-wave state versus stripe state. *Phys. Rev. Lett.* **113**, 046402 (2014). doi: 10.1103/PhysRevLett.113.046402; pmid: 25105638
19. J. P. F. LeBlanc *et al.*, Solutions of the Two-Dimensional Hubbard Model: Benchmarks and Results from a Wide Range of Numerical Algorithms. *Phys. Rev. X* **5**, 041041 (2015). doi: 10.1103/PhysRevX.5.041041
20. S. R. White, Density matrix formulation for quantum renormalization groups. *Phys. Rev. Lett.* **69**, 2863–2866 (1992). doi: 10.1103/PhysRevLett.69.2863; pmid: 10046608
21. S. R. White, Density-matrix algorithms for quantum renormalization groups. *Phys. Rev. B Condens. Matter* **48**, 10345–10356 (1993). doi: 10.1103/PhysRevB.48.10345; pmid: 10007313
22. U. Schollwöck, The density-matrix renormalization group. *Rev. Mod. Phys.* **77**, 259–315 (2005). doi: 10.1103/RevModPhys.77.259
23. Y.-F. Jiang, J. Zaanen, T. P. Devereaux, H.-C. Jiang, Ground state phase diagram of the doped Hubbard model on the four-leg cylinder. *Phys. Rev. Res.* **2**, 033073 (2020). doi: 10.1103/PhysRevResearch.2.033073
24. J. Jordan, R. Orús, G. Vidal, F. Verstraete, J. I. Cirac, Classical simulation of infinite-size quantum lattice systems in two spatial dimensions. *Phys. Rev. Lett.* **101**, 250602 (2008). doi: 10.1103/PhysRevLett.101.250602; pmid: 19113687
25. N. V. Prokof'ev, B. V. Svistunov, Polaron Problem by Diagrammatic Quantum Monte Carlo. *Phys. Rev. Lett.* **81**, 2514–2517 (1998). doi: 10.1103/PhysRevLett.81.2514
26. S. Zhang, J. Carlson, J. E. Gubernatis, Constrained path Monte Carlo method for fermion ground states. *Phys. Rev. B Condens. Matter* **55**, 7464–7477 (1997). doi: 10.1103/PhysRevB.55.7464
27. A. Georges, G. Kotliar, W. Krauth, M. J. Rozenberg, Dynamical mean-field theory of strongly correlated fermion systems and the limit of infinite dimensions. *Rev. Mod. Phys.* **68**, 13–125 (1996). doi: 10.1103/RevModPhys.68.13
28. G. Knizia, G. K.-L. Chan, Density matrix embedding: A simple alternative to dynamical mean-field theory. *Phys. Rev. Lett.* **109**, 186404 (2012). doi: 10.1103/PhysRevLett.109.186404; pmid: 23215304
29. T. Maier, M. Jarrell, T. Pruschke, M. H. Hettler, Quantum cluster theories. *Rev. Mod. Phys.* **77**, 1027–1080 (2005). doi: 10.1103/RevModPhys.77.1027
30. W. Metzner, M. Salmhofer, C. Honerkamp, V. Meden, K. Schönhammer, Functional renormalization group approach to correlated fermion systems. *Rev. Mod. Phys.* **84**, 299–352 (2012). doi: 10.1103/RevModPhys.84.299
31. C.-C. Chang, S. Zhang, Spatially inhomogeneous phase in the two-dimensional repulsive Hubbard model. *Phys. Rev. B Condens. Matter* **78**, 165101 (2008). doi: 10.1103/PhysRevB.78.165101
32. M. Qin, H. Shi, S. Zhang, Coupling quantum Monte Carlo and independent-particle calculations: Self-consistent constraint for the sign problem based on the density or the density matrix. *Phys. Rev. B Condens. Matter* **94**, 235119 (2016). doi: 10.1103/PhysRevB.94.235119
33. B.-X. Zheng *et al.*, Stripe order in the underdoped region of the two-dimensional Hubbard model. *Science* **358**, 1155–1160 (2017). doi: 10.1126/science.aam7127; pmid: 29191901
34. A. Damascelli, Z. Hussain, Z.-X. Shen, Angle-resolved photoemission studies of the cuprate superconductors. *Rev. Mod. Phys.* **75**, 473–541 (2003). doi: 10.1103/RevModPhys.75.473
35. O. Andersen, A. Liechtenstein, O. Jepsen, F. Paulsen, LDA energy bands, low-energy hamiltonians, t′, t″, $t_\perp$ (k), and $J_\perp$. *J. Phys. Chem. Solids* **56**, 1573–1591 (1995) Proceedings of the Conference on Spectroscopies in Novel Superconductors. doi: 10.1016/0022-3697(95)00269-3
36. M. Hirayama, Y. Yamaji, T. Misawa, M. Imada, *Ab initio* effective Hamiltonians for cuprate superconductors. *Phys. Rev. B Condens. Matter* **98**, 134501 (2018). doi: 10.1103/PhysRevB.98.134501
37. See supplementary materials.
38. A better proxy for T_c might be the magnitude of the superconducting gap. This would be more difficult to calculate, and it also is only roughly tied to T_c.
39. V. J. Emery, S. A. Kivelson, Importance of phase fluctuations in superconductors with small superfluid density. *Nature* **374**, 434–437 (1995). doi: 10.1038/374434a0
40. D. J. Scalapino, A common thread: The pairing interaction for unconventional superconductors. *Rev. Mod. Phys.* **84**, 1383–1417 (2012). doi: 10.1103/RevModPhys.84.1383
41. E. W. Huang, C. B. Mendl, H.-C. Jiang, B. Moritz, T. P. Devereaux, Stripe order from the perspective of the Hubbard model. *NPJ Quantum Mater.* **3**, 22 (2018). doi: 10.1038/s41535-018-0097-0
42. J. M. Tranquada, B. J. Sternlieb, J. D. Axe, Y. Nakamura, S. Uchida, Evidence for stripe correlations of spins and holes in copper oxide superconductors. *Nature* **375**, 561–563 (1995). doi: 10.1038/375561a0
43. J. M. Tranquada, Cuprate superconductors as viewed through a striped lens. *Adv. Phys.* **69**, 437–509 (2020). doi: 10.1080/00018732.2021.1935698
44. S. Jiang, D. J. Scalapino, S. R. White, Ground-state phase diagram of the *t*-*t*′-*J* model. *Proc. Natl. Acad. Sci. U.S.A.* **118**, e2109978118 (2021). doi: 10.1073/pnas.2109978118; pmid: 34706937
45. S. Gong, W. Zhu, D. N. Sheng, Robust d-Wave Superconductivity in the Square-Lattice t-J Model. *Phys. Rev. Lett.* **127**, 097003 (2021). doi: 10.1103/PhysRevLett.127.097003; pmid: 34506200
46. H.-C. Jiang, S. A. Kivelson, High Temperature Superconductivity in a Lightly Doped Quantum Spin Liquid. *Phys. Rev. Lett.* **127**, 097002 (2021). doi: 10.1103/PhysRevLett.127.097002; pmid: 34506188
47. H.-C. Jiang, S. A. Kivelson, D.-H. Lee, Superconducting valence bond fluid in lightly doped eight-leg t − J cylinders. *Phys. Rev. B Condens. Matter* **108**, 054505 (2023). doi: 10.1103/PhysRevB.108.054505
48. X. Lu, F. Chen, W. Zhu, D. N. Sheng, S.-S. Gong, Emergent Superconductivity and Competing Charge Orders in Hole-Doped Square-Lattice t-J Model. *Phys. Rev. Lett.* **132**, 066002 (2024). doi: 10.1103/PhysRevLett.132.066002; pmid: 38394594
49. H.-C. Jiang, T. P. Devereaux, Superconductivity in the doped Hubbard model and its interplay with next-nearest hopping t′. *Science* **365**, 1424–1428 (2019). doi: 10.1126/science.aal5304; pmid: 31604270
50. C.-M. Chung, M. Qin, S. Zhang, U. Schollwöck, S. R. White, Plaquette versus ordinary d -wave pairing in the t′ -Hubbard model on a width-4 cylinder. *Phys. Rev. B Condens. Matter* **102**, 041106 (2020). doi: 10.1103/PhysRevB.102.041106
51. C.-C. Chang, S. Zhang, Spin and charge order in the doped hubbard model: Long-wavelength collective modes. *Phys. Rev. Lett.* **104**, 116402 (2010). doi: 10.1103/PhysRevLett.104.116402; pmid: 20366491
52. H. Xu, H. Shi, E. Vitali, M. Qin, S. Zhang, Stripes and spin-density waves in the doped two-dimensional Hubbard model: Ground state phase diagram. *Phys. Rev. Res.* **4**, 013239 (2022). doi: 10.1103/PhysRevResearch.4.013239
53. S. R. White, D. J. Scalapino, Competition between stripes and pairing in a t − t′ − J model. *Phys. Rev. B Condens. Matter* **60**, R753–R756 (1999). doi: 10.1103/PhysRevB.60.R753
54. E. Fradkin, S. A. Kivelson, J. M. Tranquada, *Colloquium* : Theory of intertwined orders in high temperature superconductors. *Rev. Mod. Phys.* **87**, 457–482 (2015). doi: 10.1103/RevModPhys.87.457
55. C. Lin, F. H. Zong, D. M. Ceperley, Twist-averaged boundary conditions in continuum quantum Monte Carlo algorithms. *Phys. Rev. E Stat. Nonlin. Soft Matter Phys.* **64**, 016702 (2001). doi: 10.1103/PhysRevE.64.016702; pmid: 11461437
56. M. Qin, H. Shi, S. Zhang, Benchmark study of the two-dimensional Hubbard model with auxiliary-field quantum Monte Carlo method. *Phys. Rev. B Condens. Matter* **94**, 085103 (2016). doi: 10.1103/PhysRevB.94.085103
57. Y. Gannot, S. A. Kivelson, How quantum phases on cylinders approach the two-dimensional limit. *Phys. Rev. B Condens. Matter* **107**, 075127 (2023). doi: 10.1103/PhysRevB.107.075127
58. Z. Chen *et al.*, Anomalously strong near-neighbor attraction in doped 1D cuprate chains. *Science* **373**, 1235–1239 (2021). doi: 10.1126/science.abf5174; pmid: 34516788
59. S. Jiang, D. J. Scalapino, S. R. White, Density matrix renormalization group based downfolding of the three-band Hubbard model: Importance of density-assisted hopping. *Phys. Rev. B Condens. Matter* **108**, L161111 (2023). doi: 10.1103/PhysRevB.108.L161111
60. M. Fishman, S. R. White, E. M. Stoudenmire, The ITensor Software Library for Tensor Network Calculations. *SciPost Phys. Codebases* **4** (2022). doi: 10.21468/SciPostPhysCodeb.4

61. C. Hubig *et al*., The SyTen toolkit (2017); https://syten.eu.
62. H. Xu *et al*., chiaminchung/SupplementaryData_Science2024adh7691: Supplementary Data, Version 1.1, Zenodo (2024); https://doi.org/10.5281/zenodo.10790220

ACKNOWLEDGMENTS

We thank A. Georges, S. Kivelson, A. J. Millis, M. Morales, H. Shi, E. Vitali, and T. Xiang for discussions. We are grateful to L. Reading-Ikkanda for help with graphics. H.X. thanks the Center for Computational Quantum Physics, Flatiron Institute for support and hospitality. The Flatiron Institute is a division of the Simons Foundation. **Funding:** This work was supported by the National Key Research and Development Program of the Ministry of Science and Technology (MOST) of China (2022YFA1405400 to M.Q.), the Innovation Program for Quantum Science and Technology (2021ZD0301902 to M.Q.), the National Natural Science Foundation of China (12274290 to M.Q.), and sponsorship from Yangyang Development Fund (to M.Q.); the NSF (DMR-2110041 to S.R.W.); Deutsche Forschungsgemeinschaft (DFG, German Research Foundation) under Germany's Excellence Strategy (EXC-2111 – 390814868 to U.S.); and MOST (111-2112-M-110-006-MY3 to C.-M.C.) and the Yushan Young Scholar Program under the Ministry of Education (MOE) in Taiwan (to C.-M.C.). **Author contributions:** C.-M.C., M.Q., U.S., S.R.W., and S.Z. conceptualized the work. H.X. and C.-M.C. performed computations and collected data with help from all authors. All authors contributed to the analysis of the results and writing of the manuscript. **Competing interests:** The authors declare that they have no competing interests. **Data and materials availability:** All data and code used in the analyses are available in the main text, the supplementary materials, and in the repository (*62*).

SUPPLEMENTARY MATERIALS

science.org/doi/10.1126/science.adh7691
Supplementary Text
Figs. S1 to S11
Table S1
References (*63*–*64*)

Submitted 13 March 2023; resubmitted 16 October 2023
Accepted 27 March 2024
10.1126/science.adh7691